AZIMUTH NONLINEAR CHIRP SCALING INTEGRATED WITH RANGE CHIRP SCALING ALGORITHM FOR HIGHLY SQUINTED SAR IMAGING

Qinglin Zhai[*], Wei Wang, Jiemin Hu, and Jun Zhang

College of Electronic Science and Engineering, National University of Defense Technology, Changsha 410073, China

Abstract—The difficulty of focusing high-resolution highly squinted SAR data comes from the serious azimuth-range coupling, which needs to be compensated in the procedure of imaging. Generally, the linear range walk correction (LRWC) can reduce the coupling effectively, however, it also induces the problem of azimuth-dependence of residual range cell migration (RCM) and quadratic phase. A novel algorithm is proposed to solve this problem in this paper. In this algorithm, the azimuth nonlinear chirp scaling (ANCS) operation is used, which can not only eliminate the azimuth space variation of residual RCM and frequency modulation (FM) rate but also remove the azimuth misregistration. In addition, the range chirp scaling operation is applied to correct the range-dependent RCM. After implementing the unified RCM correction, range compression and azimuth compression sequentially, the focused SAR image is acquired finally. The experimental results with simulated data demonstrate that the proposed algorithm outperforms the existing algorithms.

1. INTRODUCTION

SAR (synthetic aperture radar) [1, 2] can provide high resolution images of remote region at all times and in all weather conditions, which makes it widely applied in military fields such as missile guidance and civil fields such as landform observation. In general, SAR works in broadside mode, i.e., the antenna beam is pointed perpendicularly to the flight path of the platform. However, missile-borne SAR should work in squint mode [3] to acquire target information in front of the platform, and squinting may also increase the flexibility with which

a desired area on a surface is imaged within a single pass of the platform [4]. However, the processing of SAR echo in squint mode is more difficult than that in the broadside mode and the difficulty mainly comes from higher order range-azimuth coupling terms in the phase of the SAR transfer function [4–6]. Some algorithms for squint mode SAR involve modified range Doppler algorithm (RDA) [7], chirp scaling algorithm (CSA) [8–10], range migration algorithm (RMA) [11, 12], and azimuth nonlinear chirp scaling (ANCS) algorithm [13–17].

The standard RDA can only process broadside and small squint SAR data, and its interpolation operation is not efficient. When secondary range compression (SRC) is applied, RDA can accommodate moderate squint mode. However, at higher squint the range dependence of SRC becomes significant, and the neglecting of this dependence will make resolution broadened and sidelobe level increased on the edge of the range swath. The CSA is more efficient because the procedure only contains fast Fourier transform and complex multiplication, but the performance of high squint angle is also confined by neglecting the range dependence of SRC. A nonlinear chirp scaling algorithm is proposed in [4], where the range dependence of SRC is removed by incorporating a small nonlinear frequency modulated (FM) signal into the received range signal. In theory, the RMA is able to process the SAR data collected from any squint angle, but the Stolt interpolation operation in 2-D spectrum domain makes it impractical. In the algorithms mentioned above, SAR data is directly processed in range-Doppler domain or 2-D spectrum domain, so high pulse repetition frequency (PRF) is required to avoid the ambiguity of Doppler frequency. As a result, the high computational burden of these algorithms reduces the imaging efficiency.

In [5], the LRWC is firstly applied to remove the linear component of the RCM and to reduce the range-azimuth coupling, however, it causes the problem of azimuth focusing depth which will restrict the imaging area. Two methods are available to account for this problem, including the method of subaperture [5] and the method of ANCS. Generally, the method of ANCS is more efficient than the method of subaperture and several algorithms using ANCS are proposed. In [13] and [16], a cubic phase perturbation function is applied to equalize the FM rates of all targets at the same range gate. However, additional interpolation is required to eliminate the image misregistration. A modified ANCS operation is adopted in [15], and the image with better accuracy and little misregistration is obtained. However, it should divide the whole range swath into blocks satisfying that in each block the residual RCM is approximately range independent. As a result, the computational complexity increases. In [14], the residual

RCMC is firstly implemented, however, the azimuth-dependence of RCM is neglected, thus leading the lower accuracy of RCMC towards the azimuth edge.

In this paper, the azimuth-dependence and range-dependence of RCM are both considered. After performing the LRWC operation, a third-order azimuth filter and a nonlinear perturbation function are both applied to eliminate the azimuth-dependence of RCM and to equalize the azimuth FM rates in each range gate. Then, implementing the CS operation in range-Doppler domain removes the range-dependence of RCM, thus facilitating the overall RCMC. The proposed algorithm can not only avoid segment division in range or azimuth direction, but also eliminate the image misregistration.

This paper is organized as follows. Section 2 analyzes the characteristic of signal coupling in 2-D spectrum domain after LRWC. A modified algorithm of ANCS integrated with CS (ANCS-CS) is presented in Section 3. Some simulation results of different methods are compared in Section 4 and we give conclusion in Section 5 finally.

2. ANALYSIS OF SIGNAL COUPLING

The general geometry relationship of the squint mode SAR is shown in Fig. 1. The platform travels along its course at an altitude of H with a constant velocity V and the radar transmits and receives pulses
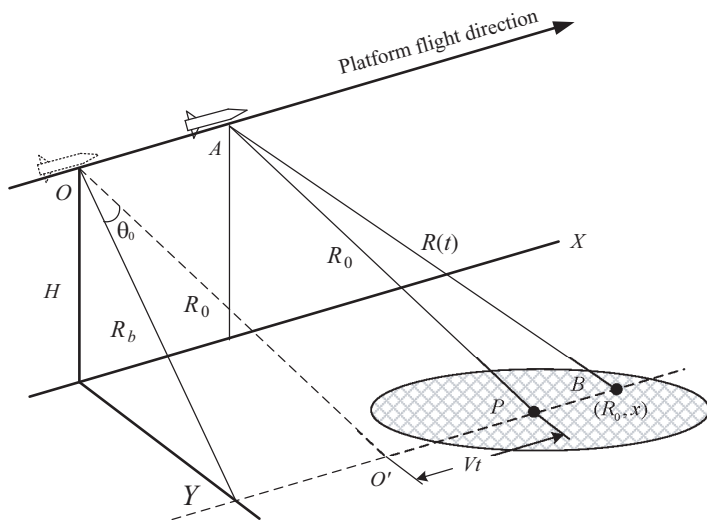

Figure 1. The geometry of the squint mode SAR.

with a squint angle of θ_0. Point O is the position of the platform at slow time zero. Point O' is the footprint of O, and the slant distance between them is R_0. The coordinate of target B is defined by its slant distance R_0 and the distance between B and O', i.e., x. As shown in Fig. 1, the closest distance of target B is R_b.

At slow time t, the platform locates at point A after traveling a distance of Vt, and the center of the imaging area is P. The instantaneous slant distance of the target B can be obtained by the triangle APB, and it is expressed as

$$R(t; R_0) = \sqrt{R_0^2 + (Vt - x)^2 - 2R_0 \sin\theta_0 (Vt - x)} \qquad (1)$$

Assuming that the transmitted signal is LFM [18], with the carrier frequency f_c, chirping rate K_r, bandwidth B_r, then the echo signal after demodulation is given by

$$s_r(\tau, t; R_0) = A_0 w_r \left[\tau - \frac{2R(t)}{c} \right] w_a(t) \exp\left\{ -\frac{j4\pi}{\lambda} R(t) \right\}$$
$$\cdot \exp\left\{ j\pi K_r \left(\tau - \frac{2R(t)}{c} \right)^2 \right\} \qquad (2)$$

where τ is the fast time, λ the wavelength, c the velocity of light, and $w_r(\cdot)$ and $w_a(\cdot)$ are the range window and azimuth window, respectively.

After Taylor expansion, the instantaneous slant distance $R(t; R_0)$ can be approximately as [19]

$$R(t; R_0) \approx \sqrt{R_0^2 + V^2 \cos^2\theta_0 \left(t - \frac{x}{V} \right)^2}$$
$$- \sin\theta_0 V \left(t - \frac{x}{V} \right) + \frac{V^3 \cos^2\theta_0 \sin\theta_0}{2R_0^2} \left(t - \frac{x}{V} \right)^3 \quad (3)$$

By substituting (3) into (2) and applying Fourier transform in range direction, the result is

$$s(f_r, t; R_0)$$
$$= A_0 W_r(f_r) w_a(t) \exp\left\{ -\frac{j4\pi(f_c + f_r)}{c} x \sin\theta_0 \right\} \exp\left\{ -j\pi \frac{f_r^2}{K_r} \right\}$$
$$\cdot \exp\left\{ \frac{j4\pi(f_c + f_r)}{c} V t \sin\theta_0 \right\}$$
$$\exp\left\{ -\frac{j4\pi(f_c + f_r)}{c} \sqrt{R_0^2 + V^2 \cos^2\theta_0 \left(t - \frac{x}{V} \right)^2} \right\}$$
$$\cdot \exp\left\{ -\frac{j4\pi(f_c + f_r)}{c} \frac{V^3 \cos^2\theta_0 \sin\theta_0}{2R_0^2} \left(t - \frac{x}{V} \right)^3 \right\} \qquad (4)$$

where f_r is the range frequency and $W_r(\cdot)$ the range frequency window. In (4), the second exponential term is the range FM term, and the last three exponential terms are the LRW term, the quadratic RCM term and the cubic RCM term, respectively. The LRWC function is denoted as

$$H_1(f_r, t) = \exp\left\{-\frac{j4\pi(f_c + f_r)}{c}Vt\sin\theta_0\right\} \tag{5}$$

Multiplying (4) with (5) and applying Fourier transform in azimuth direction, the signal in 2-D spectrum domain can be expressed as

$$
\begin{aligned}
&s_1(f_r, f_a; R_0)\\
&= A_0 W_r(f_r)W_a(f_a)\exp\left\{-\frac{j4\pi(f_c + f_r)}{c}x\sin\theta_0\right\}\exp\left\{-j2\pi f_a\frac{x}{V}\right\}\\
&\quad\cdot\exp\left\{-j\pi\frac{f_r^2}{K_r}\right\}\exp\left\{-\frac{j4\pi R_0}{\lambda}\sqrt{\left(1+\frac{f_r}{f_c}\right)^2 - \left(\frac{f_a\lambda}{2V'}\right)^2}\right\}\\
&\quad\cdot\exp\left\{\frac{j\pi R_0(f_c+f_r)\sin\theta_0\lambda^3 f_a^3}{4cV'^3\cos\theta_0}\left[\left(1+\frac{f_r}{f_c}\right)^2 - \left(\frac{f_a\lambda}{2V'}\right)^2\right]^{-3/2}\right\}
\end{aligned} \tag{6}
$$

where f_a is the azimuth frequency, $W_a(\cdot)$ the azimuth frequency window, and $V' = V\cos\theta_0$. It is obvious that the range-azimuth coupling in 2-D spectrum domain exist in the fourth and fifth exponential term. Let $\Phi(f_r, f_a; R_0)$ denote the summed phases of the last two terms, and it can be expanded into a power series of f_r [15] as follows

$$
\begin{aligned}
\Phi(f_r, f_a; R_0) \approx{}& \phi_0(f_a; R_0) + \phi_1(f_a; R_0)f_r\\
&+\phi_2(f_a; R_0)f_r^2 + \phi_3(f_a; R_0)f_r^3 + O(f_r^3)
\end{aligned} \tag{7}
$$

where

$$
\left\{
\begin{aligned}
\phi_0(f_a; R_0) ={}& -\frac{4\pi R_0}{\lambda}D(f_a) + \frac{\pi R_0 P_3(f_a)}{\lambda}\frac{1}{D^3(f_a)}\\
\phi_1(f_a; R_0) ={}& -\frac{4\pi R_0}{c}\frac{1}{D(f_a)} + \frac{\pi R_0 P_3(f_a)}{c}\frac{1}{D^3(f_a)}\\
&-\frac{3\pi R_0 P_3(f_a)}{c}\frac{1}{D^5(f_a)}\\
\phi_2(f_a; R_0) ={}& \frac{2\pi R_0}{cf_c}\frac{1-D^2(f_a)}{D^3(f_a)} - \frac{3\pi R_0 P_3(f_a)}{cf_c}\frac{1}{D^5(f_a)}\\
&+\frac{3\pi R_0 P_3(f_a)}{2cf_c}\frac{5-D^2(f_a)}{D^7(f_a)}\\
\phi_3(f_a; R_0) ={}& -\frac{2\pi R_0}{cf_c^2}\frac{1-D^2(f_a)}{D^5(f_a)} + \frac{3\pi R_0 P_3(f_a)}{2cf_c^2}\frac{5-D^2(f_a)}{D^7(f_a)}\\
&-\frac{5\pi R_0 P_3(f_a)}{2cf_c^2}\frac{7-3D^2(f_a)}{D^9(f_a)}
\end{aligned}
\right. \tag{8a}
$$

$$D(f_a) = \sqrt{1 - \left(\frac{f_a\lambda}{2V'}\right)^2} \tag{8b}$$

$$P_3(f_a) = \frac{\sin\theta_0 \lambda^3 f_a^3}{4V'^3 \cos\theta_0} \tag{8c}$$

In (7), $\phi_0(f_a; R_0)$ is the azimuth modulation term, $\phi_1(f_a; R_0)f_r$ represents the residual RCM after LRWC, $\phi_2(f_a; R_0)f_r^2$ is the term of SRC, and $\phi_3(f_a; R_0)f_r^3$ denotes the third order range-azimuth coupling term.

To quantificationally analyze the amount of these terms, a simulation is implemented by substituting the maximum value of range frequency and azimuth frequency into them. Considering the fact that the theoretical range resolution is determined by the bandwidth B_r and that the area of range frequency is between $-B_r/2$ and $B_r/2$ after signal demodulation if the over sampling rate in the fast time domain is 1. Then, the maximum value of range frequency equals to $-c/(4\rho_r)$, where ρ_r denotes the theoretical range resolution. Also, the theoretical azimuth resolution is determined by the Doppler bandwidth B_a and that the area of Doppler frequency is between $-B_a/2$ and $B_a/2$ after linear range walk correction if the over sampling rate in the slow time domain is 1. As a result, the maximum value of azimuth frequency equals to $-V/(2\rho_a)$, where ρ_a is the theoretical azimuth resolution. In the simulation, ρ_r and ρ_a is 1 m, the closest distance of the target is 20 km, and the flight velocity of the platform is 1000 m/s. Fig. 2 shows the diagrams for the term SRC and the third order range-azimuth coupling term under various squint angles.

From the quantitative simulation, it is obvious that both coupling terms become more serious as the squint angle increase under the same carrier frequency. The third order coupling term is 3 orders of magnitude smaller than SRC, indicating that the cubic phase is negligible. However, the SRC term should be compensated in high-resolution highly squinted SAR imaging, and we can set the coefficient of $\phi_2(f_a; R_0)$ at the reference slant range R_{ref} because the range-dependence of SRC is weak.

On the basis of aforementioned analysis, the new type of (6) can be rewritten as

$$s_1(f_r, f_a; R_0)$$
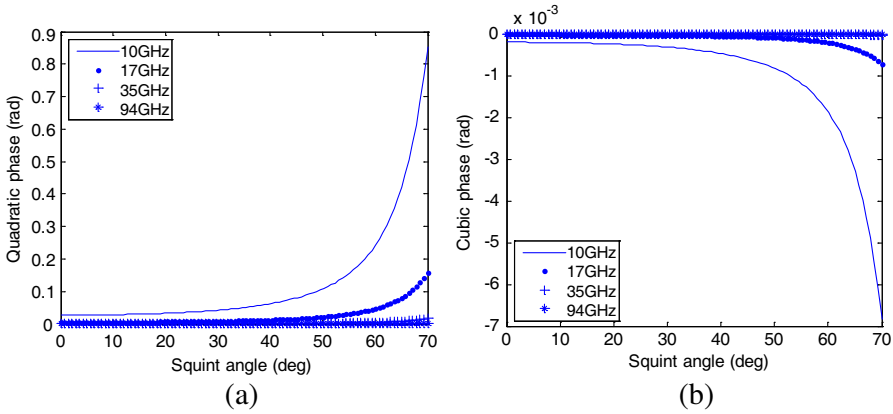$$\approx A_0 W_r(f_r)W_a(f_a)\exp\left\{-\frac{j4\pi(f_c + f_r)}{c}x\sin\theta_0\right\}\exp\left\{-j2\pi f_a\frac{x}{V}\right\}$$

Figure 2. (a) Curves for the term SRC and (b) the third order range-azimuth coupling term under various squint angles.

$$\cdot \exp\left\{-j\pi \frac{f_r^2}{K_r}\right\} \exp\{j\phi_0(f_a; R_0)\}$$

$$\exp\{j\phi_1(f_a; R_0)f_r\} \exp\{j\phi_2(f_a; R_{ref})f_r^2\}$$

$$= A_0 W_r(f_r) W_a(f_a) \exp\left\{-\frac{j4\pi(f_c + f_r)}{c} x \sin\theta_0\right\} \exp\left\{-j2\pi f_a \frac{x}{V}\right\}$$

$$\cdot \exp\{j\phi_0(f_a; R_0)\} \exp\{j\phi_1(f_a; R_0)f_r\} \exp\left\{-j\frac{\pi}{K_m(f_a)} f_r^2\right\} \quad (9)$$

where $K_m(f_a)$ is the integrated FM rate and it satisfies $1/K_m(f_a) = 1/K_r - \phi_2(f_a, R_{ref})/\pi$.

3. ANCS INTEGRATED WITH CS ALGORITHM

The LRWC can correct the linear migration of the target effectively. However, there is still some residual RCM which should be compensated in the afterward procedure. In addition, the LRWC also induces the problem of azimuth-dependence of RCM and azimuth quadratic phase. Therefore, the method of ANCS is applied to eliminate the azimuth variation component of residual RCM and azimuth FM rates in each range gate. Then, the CS operation is performed in the range-Doppler domain to remove the range-dependence of residual RCM. After implementing the unified residual RCMC, range compression and azimuth compression, the focused SAR image can be acquired finally. The details are presented as follows.

3.1. ANCS Operation

Using the range inverse Fourier transform, the signal in (9) is turned to

$$s_2(\tau, f_a; R_0) \approx A_0 w_r(\tau) W_a(f_a) \exp\left\{-\frac{j4\pi}{\lambda} x \sin\theta_0\right\}$$

$$\exp\left\{j\pi K_m(f_a)\left(\tau - \frac{2}{c}x\sin\theta_0 + \frac{\phi_1(f_a, R_0)}{2\pi}\right)^2\right\}$$

$$\cdot \exp\left\{-j2\pi f_a \frac{x}{V}\right\} \exp\left\{j\phi_0(f_a; R_0)\right\} \quad (10)$$

The last exponential term in (10) denotes azimuth modulation, which can be expanded into a power series of f_a, and the result is

$$\phi_0(f_a; R_0) \approx -\frac{4\pi R_0}{\lambda} - \frac{\pi}{K_a} f_a^2 + \sum_{n=3}^{\infty} \psi_n f_a^n \quad (11)$$

where $K_a = -2V^2 \cos^2\theta_0/\lambda R_0$ is the azimuth FM rate at slant range R_0. From (10) it is observed that the slant range of a target with the coordinate (R_0, x) will become $R_0 + x\sin\theta_0$, so the targets that have different initial slant ranges may lie in the same range cell. If the azimuth compression is processed with a filter with FM rate K_a, the error of the FM rate will lead to azimuth defocusing toward the azimuth edge. This is the problem of focusing depth caused by LRWC.

Let R_s denote $R_0 + V t_x \sin\theta_0$, where $t_x = x/V$. Then the azimuth FM rate K_a can be approximated to the linear form of t_x as

$$K_a \approx -\frac{2V^2\cos^2\theta_0}{\lambda R_s} - \frac{2V^3\cos^2\theta_0\sin\theta_0}{\lambda R_s^2} t_x$$

$$= K_{aref} + K_{SAC} t_x \quad (12)$$

In (10), the term $\phi_1(f_a, R_0)/2\pi$ contains the original slant range and the residual RCM of the target, and it can be further represented as

$$\frac{\phi_1(f_a, R_0)}{2\pi} = -\frac{2R_0}{c} - \frac{2R_0}{c}\left(\frac{1}{D(f_a)} - 1\right) + \frac{R_0 P_3(f_a)}{2c}\frac{1}{D^3(f_a)}$$

$$-\frac{3R_0 P_3(f_a)}{2c}\frac{1}{D^5(f_a)} = -\frac{2}{c}R_0 - \frac{2}{c}\alpha(f_a)R_0 \quad (13)$$

where $\alpha(f_a) = \frac{1}{D(f_a)} - 1 - \frac{P_3(f_a)}{4D^3(f_a)} + \frac{3P_3(f_a)}{4D^5(f_a)}$ denotes the coefficient of the residual RCM which is relevant to the azimuth frequency. Substituting

(11) and (13) into (10) yields

$$s_3(\tau, f_a; R_s) = A_0 w_r(\tau) W_a(f_a) \exp\left\{-\frac{j4\pi x R_s}{\lambda}\right\}$$

$$\exp\left\{j\pi K_m(f_a)\left(\tau - \frac{2}{c}R_s - \frac{2}{c}\alpha(f_a)R_0\right)^2\right\}$$

$$\cdot \exp\left\{-j2\pi f_a \frac{x}{V}\right\}\exp\left\{-j\pi \frac{f_a^2}{K_a}\right\}\exp\left\{j\sum_{n=3}^{\infty}\psi_n f_a^n\right\} \quad (14)$$

From (14), we can find that the targets in the same range gate have various curves of RCM if they have different original slant ranges. It will cause the error of RCMC toward the edge of azimuth if a unified RCMC is applied in each range gate. Moreover, the third and higher order terms of f_a can be compensated by multiplying with their conjugate, so the compensation function is

$$H_2(f_a; R_0) = \exp\left\{-j\sum_{n=3}^{\infty}\psi_n f_a^n\right\}$$

$$= \exp\left\{-j\left[\phi_0(f_a; R_0) + \frac{4\pi R_0}{\lambda} + \frac{\pi}{K_a}f_a^2\right]\right\} \quad (15)$$

Multiplying (14) with (15) results

$$s_4(\tau, f_a; R_s)$$

$$\approx A_0 w_r(\tau) W_a(f_a) \exp\left\{-\frac{j4\pi}{\lambda}R_s\right\} \exp\left\{j\pi K_m(f_a)\left(\tau - \frac{2}{c}R_s\right.\right.$$

$$\left.\left. - \frac{2}{c}\alpha(f_a)R_0\right)^2\right\} \cdot \exp\left\{-j2\pi f_a \frac{x}{V}\right\} \exp\left\{-j\pi \frac{f_a^2}{K_a}\right\} \quad (16)$$

Before employing the ANCS operation, an extra cubic azimuth filter is needed [14], which can be expressed as

$$H_3(f_a) = \exp\left\{j\pi Y_3 f_a^3\right\} \quad (17)$$

Applying the range Fourier transform and azimuth inverse Fourier transform to the filtered signal yields

$$s_5(f_r, t; R_s) = A_0 W_r(f_r) w_a(t) \exp\left\{-\frac{j4\pi}{\lambda}R_s\right\}\exp\left\{-j\pi\frac{4R_s}{c}f_r\right\}$$

$$\exp\left\{-j\frac{\pi}{K_m(f_a)}f_r^2\right\} \cdot \exp\left\{-j\pi\frac{4\alpha(f_a)R_0}{c}f_r\right\}$$

$$\exp\left\{j\pi K_a(t - t_x)^2\right\}\exp\left\{j\pi Y_3 K_a^3(t - t_x)^3\right\} \quad (18)$$

A chirp scaling factor with cubic phase is introduced to eliminate the azimuth-dependence of the residual RCM and the azimuth-dependence of the FM rate, and the factor can be presented as

$$H_4(t) = \exp\left\{j\pi q_2 t^2 + j\pi q_3 t^3\right\} \tag{19}$$

After multiplying (19) with (18) and applying the azimuth Fourier transformation, the signal in 2-D spectrum domain can be expressed as

$$
\begin{aligned}
& s_6(f_r, f_a; R_s) \\
= {} & A_0 W_r(f_r) W_a\left(\frac{f_a - t_x q_2}{K_a + q_2}\right) \exp\left\{-\frac{j4\pi}{\lambda} R_s\right\} \exp\left\{-j\pi \frac{4R_s}{c} f_r\right\} \\
& \cdot \exp\left\{-j\pi \frac{4\alpha(f_a) R_0}{c} f_r\right\} \exp\left\{-j\frac{\pi}{K_m(f_a)} f_r^2\right\} \exp\left\{-j2\pi \frac{f_a + K_a t_x}{K_a + q_2} f_a\right\} \\
& \cdot \exp\left\{j\frac{\pi}{(K_a + q_2)^2}\left[K_a(f_a - q_2 t_x)^2 + q_2(f_a + K_a t_x)^2\right]\right\} \\
& \cdot \exp\left\{j\frac{\pi}{(K_a + q_2)^3}\left[Y_3 K_a^3(f_a - q_2 t_x)^3 + q_3(f_a + K_a t_x)^3\right]\right\} \tag{20}
\end{aligned}
$$

Let $\Phi(f_a)$ denote the summation of the last three phases in (20). We can find that $\Phi(f_a)$ is relevant to the azimuth position and azimuth modulation of the target, then it can be expanded to a power series of t_x and f_a as

$$
\begin{aligned}
\Phi(f_a) = {} & A(q_2, q_3, Y_3, f_a, f_a^2, f_a^3) + B(q_2, q_3, Y_3) t_x f_a \\
& + C(q_2, q_3, Y_3) t_x^2 f_a + D(q_2, q_3, Y_3) t_x f_a^2 \\
& + \phi(q_2, q_3, Y_3, t_x, t_x^2, t_x^3) \tag{21}
\end{aligned}
$$

In (21), the first term is the azimuth-independent modulation, which can be compensated in azimuth compression. The second term denotes the azimuth position of the target. The third term represents the azimuth distortion, which should be eliminated. The fourth term stands the azimuth dependence on the azimuth FM, and the last one refers to the summation of all of the other remained terms which can be neglected in the following processing. The coefficients of these terms are showed as

$$A\left(q_2, q_3, Y_3, f_a, f_a^2, f_a^3\right) = -\pi\frac{f_a^2}{K_{aref} + q_2} + \pi\frac{Y_3 K_{aref}^3 + q_3}{(K_{aref} + q_2)^3} f_a^3 \tag{22a}$$

$$B\left(q_2, q_3, Y_3\right) = -\frac{2\pi K_{aref}}{K_{aref} + q_2} \tag{22b}$$

$$C(q_2, q_3, Y_3)$$
$$= \pi \frac{K_{aref}\left[3K_{aref}(q_2^2 Y_3 K_{aref} + q_3) - 2K_{SAC}q_2\left(K_{aref} + q_2\right)/K_{aref}\right]}{(K_{aref} + q_2)^3} \quad (22\mathrm{c})$$

$$D(q_2, q_3, Y_3)$$
$$= \pi \frac{K_{aref}\left[K_{SAC}\left(K_{aref} + q_2\right)/K_{aref} - 3\left(q_2 Y_3 K_{aref}^2 - q_3\right)\right]}{(K_{aref} + q_2)^3} \quad (22\mathrm{d})$$

To eliminate the azimuth distortion and azimuth dependence on azimuth FM, the coefficients $C(q_2, q_3, Y_3)$ and $D(q_2, q_3, Y_3)$ should be set to zero. Moreover, we usually set $B(q_2, q_3, Y_3)$ to $-2\pi/\beta$, where $\beta \neq 1$ is a constant. Therefore, three equations are presented as

$$\begin{cases} B(q_2, q_3, Y_3) = -2\pi/\beta \\ C(q_2, q_3, Y_3) = 0 \\ D(q_2, q_3, Y_3) = 0 \end{cases} \quad (23)$$

The parameters in (17) and (19) can be acquired from (23), showing as

$$\begin{cases} q_2 = K_{aref}(\beta - 1) \\ q_3 = K_{SAC}(\beta - 1)/3 \\ Y_3 = \dfrac{K_{SAC}(2\beta - 1)}{3K_{aref}^3(\beta - 1)} \end{cases} \quad (24)$$

By substituting (24) into (20), we can obtain the simplified signal as

$$s_7(f_r, f_a; R_s)$$
$$= A_0 W_r(f_r) W_a\left(\frac{f_a - t_x q_2}{K_a + q_2}\right) \exp\left\{-\frac{j4\pi}{\lambda}R_s\right\} \exp\left\{-j\pi\frac{4R_s}{c}f_r\right\}$$
$$\cdot \exp\left\{-j\pi\frac{4\alpha(f_a)R_s}{c}f_r\right\} \exp\left\{-j\frac{\pi}{K_m(f_a)}f_r^2\right\}$$
$$\cdot \exp\left\{-j2\pi\frac{t_x}{\beta}f_a\right\} \exp\left\{-j\pi\frac{f_a^2}{\beta K_{aref}}\right\} \exp\left\{j\pi\frac{K_{SAC}}{3K_{aref}^3\beta(\beta - 1)}f_a^3\right\} \quad (25)$$

After range Fourier transformation, the signal in range-Doppler domain is shown as

$$s_8(\tau, f_a; R_s) = A_0 w_r(\tau) W_a\left(\frac{f_a - t_x q_2}{K_a + q_2}\right) \exp\left\{-\frac{j4\pi}{\lambda}R_s\right\}$$
$$\exp\left\{j\pi K_m(f_a)\left(\tau - \frac{2}{c}R_s - \frac{2}{c}R_s\alpha(f_a)\right)^2\right\}$$

$$\cdot \exp\left\{-j2\pi\frac{t_x}{\beta}f_a\right\} \exp\left\{-j\pi\frac{f_a^2}{\beta K_{aref}}\right\} \exp\left\{j\pi\frac{K_{SAC}}{3K_{aref}^3\beta(\beta-1)}f_a^3\right\} \quad (26)$$

Inspecting Equation (26), we can find that the azimuth FM rate has been regulated to a fixed constant, which is independent of the azimuth position. Therefore, the operation of azimuth compression can be easily implemented with a fixed filter function. In addition, the azimuth distortion as well as the azimuth-dependence of the residual RCM has been eliminated. In order to facilitate the correction of the residual RCM, the range-dependence of the RCM should also be removed. And the details are presented in the next section.

3.2. CS Operation in Range Direction

The principle of CS is applied to deal with the range dependence of the residual RCM, and the chirp scaling factor is employed by

$$H_{cs}(\tau, f_a) = \exp\left\{j\pi K_m(f_a)\alpha(f_a)\left(\tau - \frac{2}{c}R_{ref} - \frac{2}{c}R_{ref}\alpha(f_a)\right)^2\right\} \quad (27)$$

After multiplying (26) with (27), the signal in range-Doppler domain can be written as

$$
\begin{aligned}
&s_9(\tau, f_a; R_s) \\
&= s_8(\tau, f_a) \cdot H_{cs}(\tau, f_a) \\
&= A_0 w_r(\tau) W_a\left(\frac{f_a - t_x q_2}{K_a + q_2}\right) \exp\left\{-\frac{j4\pi}{\lambda}R_s\right\} \exp\left\{-j2\pi\frac{t_x}{\beta}f_a\right\} \\
&\quad \exp\left\{-j\pi\frac{f_a^2}{\beta K_{aref}}\right\} \cdot \exp\left\{j\pi\frac{Y_3 K_{aref}^3 + q_3}{(K_{aref} + q_2)^3}f_a^3\right\} \\
&\quad \exp\left\{j\pi\left(1 + \alpha(f_a)\right)K_m(f_a)\left[\tau - \frac{2}{c}R_s - \frac{2}{c}R_{ref}\alpha(f_a)\right]^2\right\} \\
&\quad \cdot \exp\left\{j\Theta(f_a, R_s)\right\} \quad\quad\quad\quad\quad\quad\quad\quad\quad\quad\quad (28)
\end{aligned}
$$

where

$$\Theta(f_a, R_s) = \frac{4\pi}{c^2}K_m(f_a)\alpha(f_a)\left(1 + \alpha(f_a)\right)\left(R_s - R_{ref}\right)^2 \quad (29)$$

After the range Fourier transformation, the signal can be

expressed as

$$
\begin{aligned}
&s_{10}(f_r, f_a; R_s) \\
&= A_0 W_r(f_r) W_a\left(\frac{f_a - t_x q_2}{K_a + q_2}\right) \exp\left\{-\frac{j4\pi}{\lambda} R_s\right\} \exp\left\{-j2\pi \frac{t_x}{\beta} f_a\right\} \\
&\quad \cdot \exp\left\{-j\pi \frac{f_a^2}{\beta K_{aref}}\right\} \exp\left\{j\pi \frac{Y_3 K_{aref}^3 + q_3}{(K_{aref} + q_2)^3} f_a^3\right\} \\
&\quad \exp\left\{-j\pi \frac{f_r^2}{(1 + \alpha(f_a)) K_m(f_a)}\right\} \\
&\quad \cdot \exp\left\{-j\frac{4\pi f_r}{c}(R_s + \alpha(f_a) R_c)\right\} \exp\left\{j\Theta(f_a, R_s)\right\}
\end{aligned}
\tag{30}
$$

Therefore, a filter that performs range compression and RCMC is obtained

$$
\begin{aligned}
&H_{rc,rcmc}(f_r, f_a) \\
&= \exp\left\{j\pi \frac{f_r^2}{(1 + \alpha(f_a)) K_m(f_a)}\right\} \exp\left\{j\frac{4\pi f_r}{c} \alpha(f_a) R_{ref}\right\}
\end{aligned}
\tag{31}
$$

Multiply (30) with (31) and perform range inverse Fourier transformation, the range-compressed signal is expressed as follows

$$
\begin{aligned}
s_{11}(\tau, f_a; R_s) &= IFFT\left[s_{10}(f_r, f_a; R_s) \cdot H_{rc,rcmc}(f_r, f_a)\right] \\
&= A_0 W_a\left(\frac{f_a - t_x q_2}{K_a + q_2}\right) \mathrm{sinc}\left[B_r\left(\tau - \frac{2(R_0 + x\sin\theta_0)}{c}\right)\right] \\
&\quad \exp\left\{-\frac{j4\pi}{\lambda} R_s\right\} \exp\left\{-j2\pi \frac{t_x}{\beta} f_a\right\} \cdot \exp\left\{-j\pi \frac{f_a^2}{\beta K_{aref}}\right\} \\
&\quad \exp\left\{j\pi \frac{Y_3 K_{aref}^3 + q_3}{(K_{aref} + q_2)^3} f_a^3\right\} \exp\left\{j\Theta(f_a, R_s)\right\}
\end{aligned}
\tag{32}
$$

3.3. Azimuth Compression

On the basis of ANCS operation, range CS operation, and unified RCMC, the residual RCM has been completely removed. Also, the dependence of azimuth modulation is eliminated. Then the azimuth compress function can be easily acquired as below.

$$
H_{ac}(f_a, R_s) = \exp\left\{j\pi \frac{f_a^2}{\beta K_{aref}} - j\pi \frac{K_{SAC}}{3 K_{aref}^3 \beta(\beta - 1)} f_a^3\right\}
\tag{33}
$$

The last exponential term in (32) is the residual phase caused by CS operation, and the function for the phase compensation is presented

as

$$H_{ec}(f_a, R_s) = \exp\{-j\Theta(f_a, R_s)\}$$
$$= \exp\left\{-j\frac{4\pi}{c^2}K_m(f_a)\alpha(f_a)\left(1+\alpha(f_a)\right)\left(R_s - R_{ref}\right)^2\right\} \quad (34)$$

After azimuth compression, residual phase compensation and azimuth inverse Fourier transformation, the final focused SAR image can be obtained as

$$s_{12}(\tau, t; R_0) = A_0 \text{sinc}\left[B_r\left(\tau - \frac{2(R_0 + x\sin\theta_0)}{c}\right)\right]$$
$$\text{sinc}\left[B_a\left(t - \frac{t_x}{\beta}\right)\right]\exp\left\{-\frac{j4\pi}{\lambda}R_s\right\} \quad (35)$$

From (35), we can find that the focused position of the target is $(R_0 + x\sin\theta_0, x/\beta)$, which is offset from the actual position (R_0, x). The geometrical distortion comes from the LRWC and ANCS operation, and the method to correct this distortion is illuminated in [15].

Above all, the flow diagram of the proposed algorithm is shown in Fig. 3.
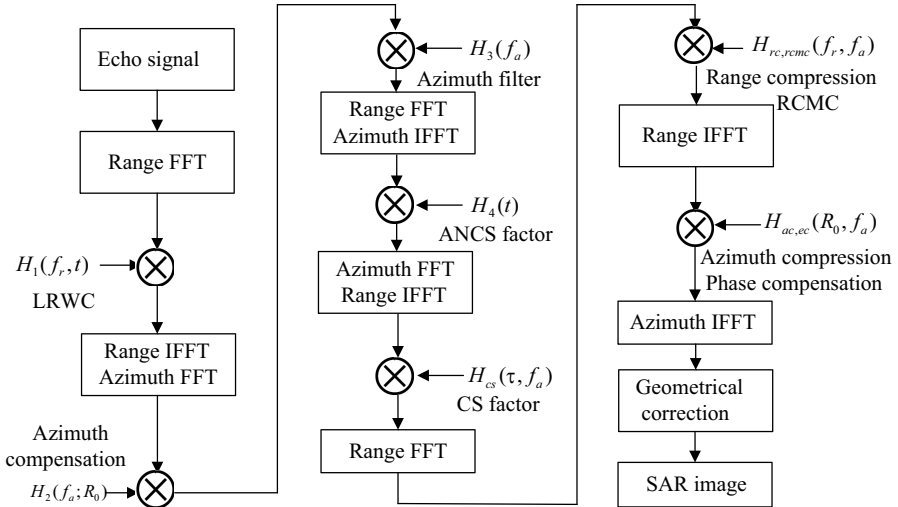

Figure 3. Flow diagram of the proposed algorithm.

4. SIMULATION RESULTS

In this section, simulated results are provided to demonstrate the performance of the proposed algorithm. The simulation parameters

are listed in Table 1 and the targets geometry is shown in Fig. 4. In this imaging plane, targets 1–5 are laid out along the direction of beam center with a distance interval of 500 meter, and the echo signal of these targets have the same azimuth time. In addition, the slant distance of target 3 is selected as the reference range, and targets 6–9 as well as target 3 locate in the perpendicularity direction of slant range, and the distance interval is 250 meter. Then the echo signal of these five targets will have the same slant range after the operation of LRWC. Two simulations are carried out to prove the effectiveness of the proposed algorithm from two aspects and the chirp scaling factor β is set to 1.1.

In the first simulation, three algorithms, i.e., NLCS algorithm [13], ENLCS algorithm [15] and the proposed algorithm are applied respectively. Fig. 5 shows the subimages of targets 3–5 after 8-time interpolating. The upper images in Fig. 5 are obtained by traditional NLCS algorithm in the presence of neglecting the quadratic range cell migration. It's obvious that all the images suffer serious distortion in azimuth direction and the distortion of the farther target is more serious. The middle images are obtained by the ENLCS algorithm, which corrects the quadratic RCM in reference range. As a result, there is residual RCM except for target 3 and a slight curve still exists in the azimuth sidelobes of target 4–5. The imaging results acquired from the proposed algorithm are shown at the bottom. It is obvious that
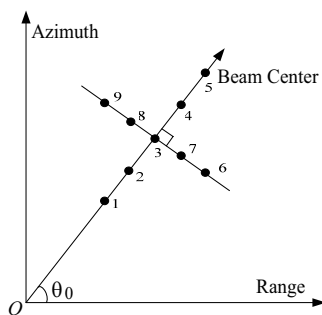

Figure 4. Targets geometry of the simulation.

Table 1. Parameters for simulation.

Carrier Frequency	10 GHz	Velocity of Platform	1000 m/s
Range Bandwidth	150 MHz	Squint Angle	60°
Pulse Repeat Frequency	600 Hz	Reference Range	20 km
Pulse Width	2.6 μs	Theoretical Resolution	1 m × 1 m

all targets are well focused since the RCM of all targets are completely corrected with range chirp scaling.

To further evaluate the performance of the proposed algorithm, the measured parameters including spatial resolution, peak sidelobe ratio (PSLR), and integrated sidelobe ratio (ISLR) are calculated, and the results are listed in Table 2. Observing Table 2, we can find that the measured parameters corresponding to the NLCS algorithm and the ENLCS algorithm become worse when the target is far from the reference range. However, nearly theoretical parameters are obtained by the proposed algorithm and the parameters keep unchangeable along the range direction.
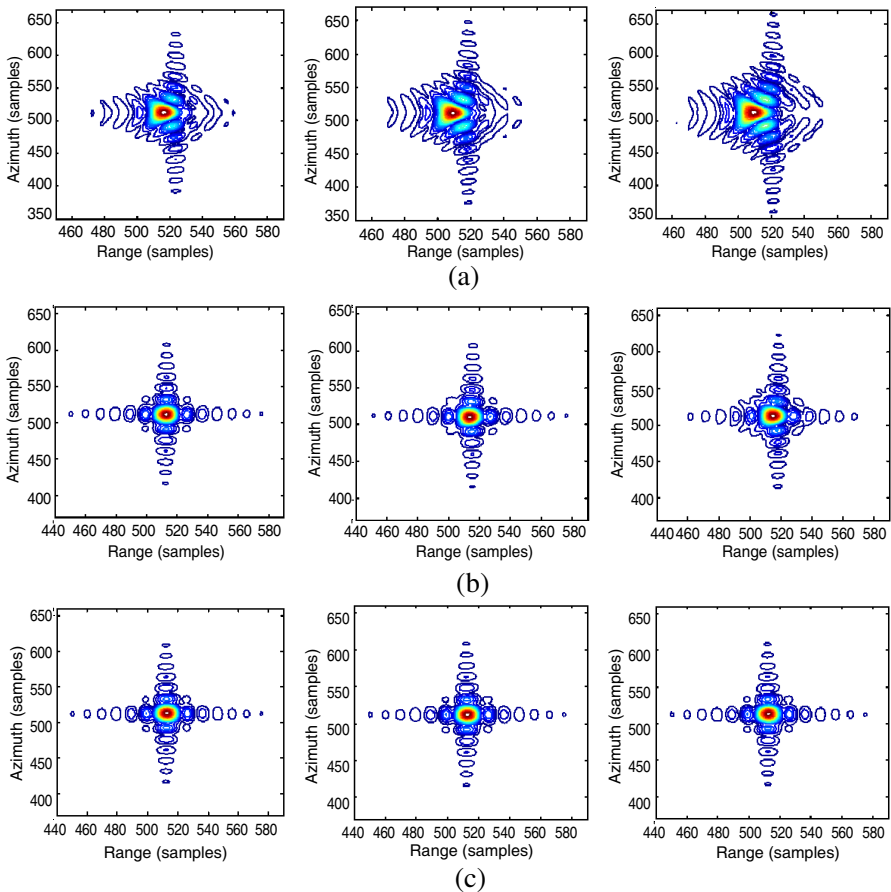

Figure 5. Simulation results of different algorithms. (a) NLCS algorithm. (b) ENLCS algorithm. (c) Proposed algorithm. The images from left to right correspond to target 3, target 4 and target 5, respectively.

In another simulation, the results obtained by the RD algorithm [7], the ANCS-based CS algorithm [14] and the proposed algorithm are compared in Fig. 6. The upper images in Fig. 6 are obtained by traditional RDA. Since the azimuth compression is performed by a unified filter, only the target at the center of the imaging scene (i.e., target 3) is well focused. As the target's distance from the scene center increases, the focusing quality degrades quickly due to the mismatching of the azimuth FM rate. The middle images are obtained by the ANCS-based CS algorithm. We can find that the phenomenon of azimuth defocusing is avoided by the operation of ANCS. However, the residual RCM is not completely corrected for

Table 2. Measured parameters of imaged targets in Fig. 5.

Algorithm	Target	Range		
		Resolution (m)	PSLR (dB)	ISLR (dB)
NLCS algorithm	Target 3	1.07	−15.71	−13.48
	Target 4	1.07	−16.54	−15.36
	Target 5	1.18	−17.02	−16.28
ENLCS algorithm	Target 3	0.95	−12.53	−10.30
	Target 4	0.95	−12.60	−10.43
	Target 5	0.95	−12.94	−10.92
Proposed algorithm	Target 3	0.95	−12.56	−10.31
	Target 4	0.95	−12.56	−10.31
	Target 5	0.95	−12.56	−10.31
Algorithm	Target	Azimuth		
		Resolution (m)	PSLR (dB)	ISLR (dB)
NLCS algorithm	Target 3	1.16	−12.40	−10.85
	Target 4	1.16	−11.41	−9.63
	Target 5	1.30	−11.05	−9.78
ENLCS algorithm	Target 3	0.92	−11.71	−9.22
	Target 4	1.01	−11.54	−9.16
	Target 5	1.14	−11.43	−9.05
Proposed algorithm	Target 3	0.92	−11.76	−9.27
	Target 4	0.92	−11.76	−9.27
	Target 5	0.92	−11.76	−9.27

that the azimuth dependence of the residual RCM is neglected. As a result, there is still a slight distortion in the images of target 8 and target 9. Observing the imaging results acquired from the proposed algorithm shown at the bottom, it's obvious that all the targets are well focused. It's convinced that the proposed algorithm improves the imaging result in both range and azimuth direction by modified ANCS operation and more accurate RCMC.

The measured parameters of the imaged targets are also
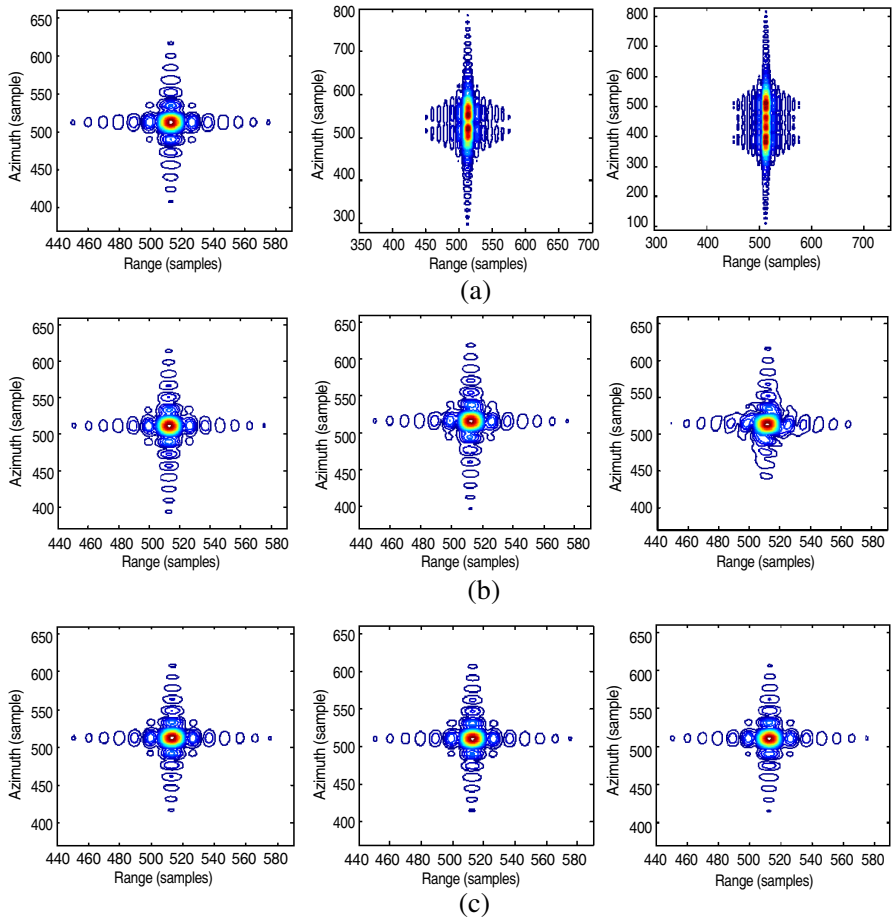

Figure 6. Simulation results of different algorithms. (a) Traditional RDA. (b) ANCS-based CS algorithm. (c) Proposed algorithm. The images from left to right correspond to target 3, target 8 and target 9, respectively.

calculated, and the results are listed in Table 3. From Table 3, it is found that the range parameters corresponding to different algorithms are approximately similar, however, the azimuth parameters various largely. For the traditional RDA, the azimuth parameters become worse as the relative distance of the target increases. Although the performance of the ANCS-based CSA improves much when compared with the traditional RDA, there is still a bit worsening in the azimuth direction. In contrast, the proposed algorithm obtains the theoretical spatial resolution, PSLR, and ISLR.

Table 3. Measured parameters of imaged targets in Fig. 6.

Algorithm	Target	Range		
		Resolution (m)	PSLR (dB)	ISLR (dB)
Traditional RDA	Target 3	0.95	−12.54	−10.29
	Target 8	0.95	−12.56	−10.28
	Target 9	0.95	−13.20	−10.29
ANCS-based CSA	Target 3	0.95	−12.52	−10.30
	Target 8	0.95	−12.73	−10.37
	Target 9	0.95	−13.01	−10.83
Proposed algorithm	Target 3	0.95	−12.53	−10.30
	Target 8	0.95	−12.47	−10.27
	Target 9	0.92	−12.11	−9.61
Algorithm	Target	Azimuth		
		Resolution (m)	PSLR (dB)	ISLR (dB)
Traditional RDA	Target 3	0.99	−12.41	−9.42
	Target 8	6.31	−5.11	−15.23
	Target 9	13.69	−2.25	−30.18
ANCS-based CSA	Target 3	1.08	−11.63	−8.39
	Target 8	1.08	−11.58	−8.49
	Target 9	1.11	−11.88	−9.56
Proposed algorithm	Target 3	0.92	−11.71	−9.22
	Target 8	0.92	−11.59	−9.94
	Target 9	0.92	−12.11	−9.61

5. CONCLUSION

For highly squinted and high resolution SAR imaging, there is serous azimuth-range coupling to be compensated. In this paper, the detailed derivation of a new ANCS algorithm and numerical simulations are presented. In the algorithm, the operation of LRWC is first performed to mitigate the signal coupling. Then, the ANCS operation is applied to eliminate the azimuth-dependence of residual RCM and FM rate. And the range chirp scaling is performed to correct the range-dependent RCM afterward. After unified RCMC, range compression and azimuth compression, the focused image is achieved, avoiding the operation of interpolation to correct azimuth misregistration. In the last, some simulation results prove the effectiveness of the proposed algorithm.

REFERENCES

1. Chan, Y. K. and V. C. Koo, "An introduction to synthetic aperture radar (SAR)," *Progress In Electromagnetics Research B*, Vol. 2, 27–60, 2008.
2. Xu, W., P. P. Huang, and Y.-K. Deng, "Multi-channel SPCMB-tops SAR for high-resolution wide-swath imaging," *Progress In Electromagnetics Research*, Vol. 116, 533–551, 2011.
3. Park, S.-H., J.-I. Park, and K.-T. Kim, "Motion compensation for squint mode spotlight SAR imaging using efficient 2D interpolation," *Progress In Electromagnetics Research*, Vol. 128, 503–518, 2012.
4. Davidson, G. W., I. G. Cumming, and M. R. Ito, "A chirp scaling approach for processing squint mode SAR data," *IEEE Trans. Aerosp. Electron. Syst.*, Vol. 32, No. 1, 121–133, Jan. 1996.
5. Yeo, T. S., N. L. Tan, C. Zhang, and Y. Lu, "A new subaperture approach to high squint SAR processing," *IEEE Trans. Geosci. Remote Sens.*, Vol. 39, No. 5, 954–968, May 2001.
6. Soumekh, M., *Synthetic Aperture Radar Signal Processing with MATLAB Algorithms*, Wiley, New York, 1999.
7. Smith, A. M., "A new approach to range-Doppler SAR processing," *Int. J. Remote Sens.*, Vol. 12, No. 2, 235–251, 1991.
8. Chen, J., J. Gao, Y. Zhu, W. Yang, and P. Wang, "A novel image formation algorithm for high-resolution wide-swath spaceborne SAR using compressed sensing on azimuth displacement phase center antenna," *Progress In Electromagnetics Research*, Vol. 125, 527–543, 2012.

9. Moreira, A. and Y.H. Huang, "Airborne SAR processing of highly squinted data using a chirp scaling approach with integrated motion compensation," *IEEE Trans. Geosci. Remote Sens.*, Vol. 32, No. 5, 1029–1040, Sep. 1994.

10. Moreira, A., J. Mittermayer, and R. Scheiber, "Extended chirp scaling algorithm for air- and spaceborne SAR data processing in stripmap and ScanSAR imaging modes," *IEEE Trans. Geosci. Remote Sens.*, Vol. 34, No. 5, 1123–1136, Sep. 1996.

11. Cumming, I. G. and F. H. Wong, *Digital Processing of Synthetic Aperture Radar Data*, Artech House, Norwood, MA, 2005.

12. Reigber, A., E. Alivizatos, A. Potsis, and A. Moreira, "Extended wavenumber-domain synthetic aperture radar focusing with integrated motion compensation," *Proc. Inst. Elect. Eng. — Radar Sonar Navig.*, Vol. 153, No. 3, 301–310, Jun. 2006.

13. Wong, F. H. and T. S. Yeo, "New applications of nonlinear chirp scaling in SAR data processing," *IEEE Trans. Geosci. Remote Sens.*, Vol. 39, No. 5, 946–953, May 2001.

14. Sun, G. C., X. W. Jiang, M. D. Xing, Z. J. Qiao, Y. R. Wu, and Z. Bao, "Focus improvement of highly squinted data based on azimuth nonlinear scaling," *IEEE Trans. Geosci. Remote Sens.*, Vol. 49, No. 6, 2308–2322, Jun. 2011.

15. An, D. X., X. T. Huang, T. Jin, and Z. M. Zhou, "Extended nonlinear chirp scaling algorithm for high-resolution highly squint SAR data focusing," *IEEE Trans. Geosci. Remote Sens.*, Vol. 50, No. 9, 3595–3609, Sep. 2012.

16. Zhang, S. X., M. D. Xing, X. G. Xia, L. Zhang, R. Guo, and Z. Bao, "Focus improvement of high-squint SAR based on azimuth dependence of quadratic range cell migration correction," *IEEE Trans. Geosci. Remote Sens.*, Vol. 10, No. 1, 150–154, Jan. 2013.

17. An, D. X., Z.-M. Zhou, X.-T. Huang, and T. Jin, "A novel imaging approach for high resolution squinted spotlight SAR based on the deramping-based technique and azimuth NLCS principle," *Progress In Electromagnetics Research*, Vol. 123, 485–508, 2012.

18. Chang, Y.-L., C.-Y. Chiang, and K.-S. Chen, "SAR image simulation with application to target recognition," *Progress In Electromagnetics Research*, Vol. 119, 35–57, 2011.

19. Huang, Y. and Z. Bao, "A new two-dimension-separated approach to high squint SAR processing," *J. Electron. Inf. Technol.*, Vol. 27, No. 1, 1–5, Jan. 2005.